Structural and Thermodynamic Properties of Nanoparticle-Protein Complexes: A Combined SAXS and SANS Study

Structural and thermodynamic properties of nanoparticle-protein complexes: a combined SAXS and SANS study

Francesco Spinozzi,[*,†] Giacomo Ceccone,[‡] Paolo Moretti,[†] Gabriele Campanella,[¶] Claudio Ferrero,[§] Sophie Combet,[‖] Isaac Ojea-Jimenez,[‡] and Paolo Ghigna[⊥]

Department of Life and Environmental Sciences, Polytechnic University of Marche, Ancona, I 60131, Italy, European Commission, Directorate General Joint Research Centre, Directorate F - Health, Consumers and Reference Materials, Consumer Products Safety Unit, Ispra, I 21027, Italy, Cornell University, Weill Medical College, New York, NY 10065, United States, ESRF - The European Synchrotron, Grenoble, F 38000, France, Laboratoire Léon-Brillouin, UMR 12 CEA-CNRS, CEA-Saclay, Gif sur Yvette, F 91191, France, and Department of Chemistry, University of Pavia, Pavia, I 27100, Italy

E-mail: f.spinozzi@univpm.it

Phone: +39 071 220 4608. Fax: +39 071 220 4316

Abstract

[*]To whom correspondence should be addressed

[†]Department of Life and Environmental Sciences, Polytechnic University of Marche, Ancona, I 60131, Italy

[‡]European Commission, Directorate General Joint Research Centre, Directorate F - Health, Consumers and Reference Materials, Consumer Products Safety Unit, Ispra, I 21027, Italy

[¶]Cornell University, Weill Medical College, New York, NY 10065, United States

[§]ESRF - The European Synchrotron, Grenoble, F 38000, France

[‖]Laboratoire Léon-Brillouin, UMR 12 CEA-CNRS, CEA-Saclay, Gif sur Yvette, F 91191, France

[⊥]Department of Chemistry, University of Pavia, Pavia, I 27100, Italy

We propose a novel method for determining structural and thermodynamic properties of nanoparticle-protein complexes in physiological conditions. The method consists in collecting a full set of small-angle X-ray and neutron scattering measurements in solutions with different concentrations of nanoparticles and protein. The nanoparticle-protein dissociation process is described in the framework of the Hill cooperative model, based on which the whole set of X-ray and neutron scattering data is fitted simultaneously. This method is applied to water solutions of gold nanoparticles in the presence of human serum albumin without any previous manipulation and can be in principle extended to all systems. We demonstrate that the protein dissociation constant, the Hill coefficient and the stoichiometry of the nanoparticle-protein complex are obtained with a high degree of confidence.

Introduction

Engineered nanomaterials (ENMs) are almost routinely used in many consumer products ranging from health and fitness to energy and food.[1] One of the most promising application areas of ENMs (particularly functionalised nanoparticles) is medicine (including both medical treatment and diagnostics).[2–6] However, although many of the peculiar properties of nanomaterials are deemed to be beneficial, there is still a wealth of concern about potential risks that ENMs may rise when in contact with humans and more in general with the environment.[7,8] As a matter of fact, a great deal of efforts are currently being made in order to understand the mechanisms governing the interactions between ENMs and cells, with special focus on engineered nanoparticles (ENPs).

Characterising the physico-chemical properties of nanomaterials and investigating their interaction with different environments are complex tasks usually addressed by using several experimental probes.[9,10] Most of these techniques can each reveal only some of the relevant properties of ENMs. In particular, information is still lacking around the effects of sample surface chemistry and composition on the behaviour of nanomaterials in different environ-

ments, and in particular in biological media.[11,12] As an example, although it is generally accepted that when nanoparticles (NPs) are put in contact with a biological medium (e.g. blood, cell culture, etc.) they are immediately covered by a layer of proteins (referred to as "protein corona"[13]), there are still several open questions concerning the interaction mechanisms and the influence of the different thermodynamic parameters.[14–19] Different methods have been used to characterise nanoparticle-protein systems.[2] Among these methods, it is worth quoting recent findings published by Bekdemir and Stellacci[20] based on analytic ultracentrifugation to determine dissociation constants, stoichiometry, and Hill coefficient for the interaction of bovine serum albumin with gold nanoparticles. Moreover, Brewer et al.[21] have also investigated the binding of serum albumin to Au NPs by means of Quartz Crystal Microbalance. Furthermore, methods based upon isolation of the protein and subsequent analysis by mass spectrometry have been also successfully used to gather information on the corona composition.[22,23] However, most of these methods are not suitable to provide information on the structural changes of the protein upon interaction with the nanoparticle.[24–26]

In the last years, microscopy techniques as well as neutron and synchrotron radiation based experimental probes have been increasingly applied to explore the interaction between nanomaterials and biological entities.[27–30] Moreover the development of advanced spectroscopy techniques such as liquid microject photoemission[31] and free electron lasers[32] will disclose new opportunities for investigating nanomaterials' reactions *in operando* or under *in situ* conditions.

In this work, the intriguing mechanism of NP-protein interactions is tackled by using concurrently small angle scattering (SAS) of X-rays and neutrons (SAXS and SANS, respectively) to inspect directly samples containing both proteins and NPs without any earlier manipulation: this allows for physiological conditions while inspecting structure and thermodynamics of the NP-protein dissociation. The SAS technique, especially SAXS, has been indeed recently reviewed and recognised to be playing a pivotal role in the investigation of *in situ* and *in operando* nanoparticle materials.[33] Our approach is as follows: first, we

simulated computationally the sensitivity of SAS to detect NP-protein dissociation for gold NPs interacting with human serum albumin (HSA). This allowed determining the "optimal" concentration ranges of NPs and protein to perform actual SAXS and SANS experiments. Then, the Hill thermodynamic model has been exploited for analysing simultaneously several sets of SAS data collected for different concentrations of both proteins and NPs using the GENFIT software.[34] The final results of the best fits are the ΔG° free energy of the NP-protein dissociation process and the mean number of proteins associated with a NP when a protein monolayer is formed, i.e. the so-called "stoichiometry" of the NP-protein interaction. The outcome of the whole set of experiments and data elaboration here described is therefore on the one hand to obtain important information on the stoichiometry of the NP-protein interaction, and on the other hand to establish an experimental protocol that can easily be transferred to other systems.

Materials and Methods

SAS Model of Protein Coated Nanoparticles

Our aim has been to study from a thermodynamic as well as a structural point of view the interactions of proteins with spherical NPs, polydisperse in size, constituted by a metal or oxide core (e.g. gold, silver, silica, etc.) and coated with a shell of stabilising materials, such as citrate anions. For this purpose, we have developed a model able to depict the main aspects of the dissociation of proteins from stabilised NPs and to describe at low resolution their structure, according to the information that can be gathered from a batch of SAXS and SANS experiments conducted on these complexes.

The Dissociation Model

We use the Hill model to describe the adsorbtion of molecules on a surface,[35] assuming that: i) protein molecules could form a monolayer on a NP; ii) a dissociation equilibrium is

established between proteins bound to a NP and free protein molecules in solution; iii) the dissociation involves n protein molecules at a time and takes places at identical association sites, the number of which is constant.

On these grounds, after the association with protein molecules, NPs can be seen as polydisperse spheres with average core radius $< R >$, coated with two layers: the first layer, of thickness t_1, is compact and built up by the stabilising molecules; the second layer, of thickness t_2, is composed by a mixture of water and protein molecules. The volume fraction filled with proteins in the second layer is variable and depends on the thermodynamic equilibrium of dissociation of a number n of protein molecules (L) bound to n association sites (S) above the surface of the first layer, according to the following elementary Hill process

$$\frac{1}{n}\mathrm{L}_n\mathrm{S}_n \;\rightleftharpoons\; \mathrm{L} + \frac{1}{n}\mathrm{S}_n \tag{1}$$

The Hill coefficient n describes the cooperativity of the protein binding: if $n > 1$ once a protein is bound to the NP its affinity for binding other proteins increases, whereas for $0 < n < 1$ the affinity to other proteins decreases after the binding with the first protein. For $n = 1$ there is no cooperativity effect and the sites behave independently, according to the classical Langmuir model.[36] The Hill process (Equation 1) is described by the dissociation equilibrium constant $K_D = e^{-\Delta G^\circ/(k_B T)} = C_\mathrm{L} {C_{\mathrm{S}_n}}^{1/n} / {C_{\mathrm{L}_n\mathrm{S}_n}}^{1/n}$, which depends on the molar concentrations of n-protein-occupied sites ($C_{\mathrm{L}_n\mathrm{S}_n}$), on the free proteins in solution (C_L) and free n-sites (C_{S_n}). The corresponding reference dissociation Gibbs free energy difference is ΔG°, k_B and T being the Boltzmann constant and the absolute temperature, respectively.

The structural properties of proteins and NPs are included in the thermodynamic model as follows. First, we consider each protein molecule attached to the NP as forming a "protein box" with average basis surface a_L and height t_2. The number of protein association sites (N_max) over the NP is therefore determined by dividing the surface a_NP of the polydisperse stabilised NP by a_L. By assuming a log-normal distribution of the NP core radius, the

average surface of the stabilised NP is given by $a_{\rm NP} = 4\pi[<R>^2 (1+\xi^2) + 2 <R> t_1 + t_1^2]$, where ξ is the core radius dispersion, defined as $\xi^2 = <R>^{-2} (<R^2> - <R>^2)$. We then consider the mass balance equations. For the NPs the concentration of the total number of sites of association, expressed by $N_{\rm max} C_{\rm NP0}$, where $C_{\rm NP0}$ is the total concentration of the NPs, should be equal to the sum of the concentrations of free and occupied sites, according to $N_{\rm max} C_{\rm NP0} = n(C_{{\rm S}_n} + C_{{\rm L}_n{\rm S}_n})$. We notice that $C_{\rm NP0}$ is obtained by dividing the nominal concentration of metal or oxide forming the core of NPs (indicated by the symbol M) by the number $x_{\rm M}$ of the M atoms (or molecules) that, on average, are contained in one NP, $C_{\rm NP0} = C_{\rm M0}/x_{\rm M}$. The value of $x_{\rm M}$ is given by the ratio between the average volume of the log-normal polydisperse bare NP, $\nu_{\rm NP} = (4\pi/3) <R>^3 (1+\xi^2)^3$, and the molecular volume of a M-unit, $\nu_{\rm M} = M_{w{\rm M}}/(d_{\rm M} N_A)$, where $M_{w{\rm M}}$, and $d_{\rm M}$ are the molecular weight and the mass density of the M-unit, respectively, and N_A is the Avogadro constant. The mass balance for proteins, is $C_{\rm L} + nC_{{\rm L}_n{\rm S}_n} = C_{\rm L0}$, where $C_{\rm L0}$ is the total nominal protein concentration in the sample. Combining the two mass balances with the definition of association constant, the fraction of association sites occupied by protein molecules, defined as $\bar{Y} = C_{{\rm L}_n{\rm S}_n}/(C_{{\rm L}_n{\rm S}_n} + C_{{\rm S}_n})$, and the concentrations of free protein molecules in solution should satisfy to the following equations

$$K_D{}^n = \frac{1-\bar{Y}}{\bar{Y}} (C_{\rm L0} - N_{\rm max} \bar{Y} C_{\rm NP0})^n, \quad (2)$$

$$C_{\rm L} = C_{\rm L0} - N_{\rm max} \bar{Y} C_{\rm NP0}. \quad (3)$$

In general, Equation 2 can only be solved by numerical methods. According with the low-resolution structural model adopted here, $\bar{Y}$ can be also interpreted as the volume fraction of the second layer of the NP occupied by the protein boxes mentioned above. The dry protein volume fraction in each protein box is $\varphi = \nu_{\rm L}/(a_{\rm L} t_2)$, where the dry volume $\nu_{\rm L}$ of one protein molecule can be easily calculated by summing up the van der Waals volumes of all its atoms. The overall dry protein volume fraction of the second shell is hence the product $\bar{Y}\varphi$.

Scattering Length Densities

It is well known that data obtained by SAS experiments depend on both the scattering length density (SLD) of each homogeneous domain that constitutes the particles in solution and on the almost homogeneous SLD of the solvent.[37] For X-ray scattering (SAXS), the SLDs are the domain electron densities multiplied by the classical radius of the electron ($r_e = 2.8 \cdot 10^{-13}$ cm), whereas for neutron scattering (SANS), the SLDs depend on the coherent scattering lengths $b_{i\,\mathrm{coh}}$ of each i-isotopic species in the domain. It is noteworthy to underline that in the SANS case, when samples are dissolved in a mixture of D_2O and H_2O, the acidic hydrogens of the domains can be exchanged with D^+ and H^+ ions coming from the autoprotolysis of heavy and light water, respectively. Hence, due to the large difference between $b_{\mathrm{D\,coh}}$ and $b_{\mathrm{H\,coh}}$,[38] the SLD of the domains can be modified by changing the so-called "exchangeable deuteration grade", defined as the ratio between the concentration of the acidic deuterons (provided by D_2O) and the sum of the total concentrations of acidic deuterons and acidic protons, $x_{\mathrm{D}} = C_{\mathrm{D^+}}/(C_{\mathrm{D^+}} + C_{\mathrm{H^+}})$.

According to the dissociation model described above, stabilised NPs are considered as polydisperse spheres with two spherical shells of thickness t_1 and t_2, respectively, which comprise three SLD domains associated with core molecules (ρ_{M}), a compact layer of stabilising molecules (ρ_{F}) and a mixed layer of protein and water molecules (ρ_2) with protein volume fraction $\bar{Y}\varphi$. As a consequence, the SLD of the second layer can be expressed by

$$\rho_2 = \rho_{\mathrm{L}}\bar{Y}\varphi + \rho_{\mathrm{W}}(1 - \bar{Y}\varphi), \tag{4}$$

where ρ_{L} and ρ_{W} are the SLDs of protein and water, respectively.

In the SAXS case, fixed values of the four SLD domains ρ_α ($\alpha = \mathrm{M, F, L, W}$) can be easily calculated from the literature data of mass density d_α, molecular weight $M_{w\alpha}$ and atomic numbers Z_i of all the i-atoms forming the α-domain, according to $\rho_\alpha = (r_e d_\alpha N_A/M_{w\alpha}) \sum_i Z_i$.

As to SANS, in a mixed heavy/light water solvent with exchangeable deuteration grade

x_{D}, the SLD of the α-domain is given by $\rho_\alpha = \rho_{\mathrm{H}\alpha}(1-x_{\mathrm{D}})+\rho_{\mathrm{D}\alpha}x_{\mathrm{D}}$, where $\rho_{\mathrm{H}\alpha}$ is the SLD calculated with all the acidic hydrogens taken as protons according to $\rho_{\mathrm{H}\alpha} = (d_\alpha N_A/M_{w\alpha})\sum_i b_{i\,\mathrm{coh}}$ and $\rho_{\mathrm{D}\alpha}$ is the pertaining expression when all the acidic hydrogens have been substituted by deuterons.

Scattering Cross Sections

SAS experiments provide the so-called "macroscopic differential scattering cross section" $\frac{d\Sigma}{d\Omega}(q)$ (in short the scattering intensity) as a function of the modulus $q = (4\pi/\lambda)\sin\theta$ of the scattering vector $\mathbf{q}$, λ and 2θ being the radiation wavelength and the scattering angle, respectively. In the case of NPs in the presence of proteins, the scattering intensity is a combination of both form factors and partial structure factors. The form factors include the one of the NP, $P_{\mathrm{NP}}(q)$, and that of the protein molecule, $P_{\mathrm{L}}(q)$, whose relative weighting factors are dictated by the respective concentrations of NPs (C_{NP0}) and free protein molecules (C_{L}). The partial structure factors $S_{\alpha\beta}(q)$ are the Fourier transforms of the long-range correlation functions $g_{\alpha\beta}(r)$ between particles of kinds α and β (where $\alpha\beta$ stands for NP-NP, NP-L and L-L) and are weighted by $(C_\alpha C_\beta)^{1/2}$.[39] If the molar concentration of NPs is many orders of magnitude lower than the one of proteins, the only partial structure factor that may be significantly different from 1 is the one describing the L-L correlation. In these conditions, the scattering intensity can be written in the following form,

$$\frac{d\Sigma}{d\Omega}(q) \;=\; N_A[C_{\mathrm{NP0}}P_{\mathrm{NP}}(q) + C_{\mathrm{L}}P_{\mathrm{L}}(q)S(q)] + B, \tag{5}$$

where the evaluation of each term is elucidated hereafter. $P_{\mathrm{NP}}(q)$ is obtained by integrating the form factor $P_{3S}(q,R)$ of a three-density level sphere with core radius R over a log-normal distribution $f(R)$,

$$P_{\mathrm{NP}}(q) \;=\; \int dR\, f(R)\, P_{3S}(q,R) \tag{6}$$

Analytic expressions of $P_{3S}(q, R)$ can be found in literature, see for example Pedersen [40] or Glatter and Kratky [41]. Calculations can be performed via the GENFIT data analysis software. [34]

The form factor $P_{\mathrm{L}}(q)$ of a globular protein the atomic structure of which is known (e.g. through a coordinates' file deposited in the PDB - Protein Data Bank [42]) can be easily calculated by using different methods [43,44] whose basic difference consists in the way the solvation water is modelled. One of these methods, named SASMOL, [45] is included in GENFIT: the positions of the hydration water molecules are found by "embedding" the protein molecule in a tetrahedral close packed lattice (tcp) that mimics the structure of liquid water. Form factors are calculated as a function of the kind of radiation exploited (X-rays or neutrons), the exchangeable deuteration grade x_{D} (in the case of SANS) and the relative mass density d_{W} of the hydration water molecules surrounding the free protein molecules in solution.

The term $S(q)$ in Equation 5 is the "effective" structure factor defined as

$$S(q) = 1 + \frac{[F_{\mathrm{L}}(q)]^2}{P_{\mathrm{L}}(q)}[S_{\mathrm{LL}}(q) - 1] \tag{7}$$

where $F_{\mathrm{L}}(q)$ is the orientational average of the scattering amplitude of a protein molecule (determined by the SASMOL method) and $S_{\mathrm{LL}}(q)$ is the protein-protein structure factor. The function $S_{\mathrm{LL}}(q)$ implemented in GENFIT is described in terms of the mean spherical approximation (MSA) by taking into account a screening Coulombian repulsive potential and a Yukawian attractive potential via the random phase approximation (RPA). Parameters of this model are the average protein diameter D, the number z of protein net elementary charges (e), the added ionic strength I_S, the attractive energy J of two proteins in contact and the range d of the mutually attractive potential.

The additional term B in Equation 5 is a flat background, which takes into account incoherent scattering effects, particularly relevant to the case of SANS, owing to the large

incoherent scattering length of the protons. Moreover, since SANS data are typically affected by a non negligible uncertainty on q, the model scattering intensity fitting SANS data should be convoluted with the resolution function $R_{\rm av}(q', q)$, according to

$$\left\langle \frac{d\Sigma}{d\Omega}(q) \right\rangle = \int_{q-3\sigma_q}^{q+3\sigma_q} \frac{d\Sigma}{d\Omega}(q')\, R_{\rm av}(q', q)\, dq', \tag{8}$$

where σ_q is the experimentally available standard deviation of the q values. Analytic expressions of $R_{\rm av}(q', q)$ (available in the GENFIT) can be found in literature (see e.g. Pedersen et al.[46]).

Equation 5 deserves a crucial comment. When SAXS or SANS curves are recorded by only varying the nominal concentrations of NPs or proteins ($C_{\rm NP0}$ and $C_{\rm L0}$, respectively; see Equation 3) the whole set of data can be fitted by Equation 5 by a unique analysis, the main fitting parameters of which are the reference dissociation Gibbs free energy difference ΔG° and the cooperativity index n, which, together with the values of nominal concentrations, determines the value of $\bar{Y}$, according to Equation 2 and 3. On the other hand, $\bar{Y}$ is also the main variable that establishes the SLD of the second shell, according to Equation 4.

In order to make the global fit analysis of data more robust and to validate the suitability of the used PDB file, it is convenient to perform SAS measurements on proteins without NPs at different concentrations (also higher than those of the samples with NPs) and to include the resulting data in the global fit analysis. It is indeed worthwhile noticing that the best fit parameters of the protein form factor $P_{\rm L}(q)$ are shared by all SAS curves, with and without NPs.

Validation of the Method

The best way to check the reliability of the proposed method and optimize the sample conditions for our investigations has been to perform a best fit analysis of simulated SAS curves. To this purpose, we have firstly simulated several sets of SAXS and SANS curves,

assuming for each set fixed thermodynamic and structural features and varying protein and NP concentrations. We have then analysed each set of simulated curves through a unique best fit calculation and checked whether the fitting parameters describing thermodynamic and structural characteristics are similar to the ones fixed in the simulated set. This validation procedure enables one to check not only the maximum number of fitting parameters but also to quantify the sensitivity of the combined SAXS and SANS techniques to each of the parameters. Both simulations and fitting analyses have been performed using GENFIT.

All simulated curves have been calculated by assuming gold NPs with average core radius $<R>= 150$ Å and dispersion $\xi = 0.15$ stabilised with a shell of citrate anions, the thickness of which is fixed to the "effective" diameter of one citric acid molecule, $t_1 = (6\nu_{\mathrm{C}}/\pi)^{1/3}$, where $\nu_{\mathrm{C}} = M_{w\mathrm{C}}/(d_{\mathrm{C}}N_A)$, $M_{w\mathrm{C}}$ being the known molecular weight of the citric acid and d_{C} its mass density. Accordingly, we found $t_1 = 7.2$ Å. We have chosen human serum albumin (HSA) as protein typically used to study "corona" gold NPs. The protein form factor has been calculated via GENFIT on the basis of the PDB entry `1ao6`,[47] by setting the relative mass density of hydration water to $d_{\mathrm{W}} = 1.05$.[48] The dry HSA volume has been found to be $\nu_{\mathrm{L}} = 83300$ Å^3. By referring to results of Röcker et al.[16], the thickness of the protein corona shell and the surface of one protein molecule attached to the NP have been fixed to $t_2 = 33$ Å and $a_{\mathrm{L}} = 2800$ Å^2, respectively. Concerning the HSA parameters defining the partial structure factor $S_{\mathrm{LL}}(q)$, we have fixed the following parameters: $D = 60$ Å, $z = -4$ e (at neutral pH[49]), $I_S = 10$ μM, $J = 20$ k_BT and $d = 3.0$ Å. The very low value of I_S refers to a solution without added salts.

The maximum number of HSA molecules that can be attached to the polydisperse NP and the dry protein volume fraction in each protein box, calculated on the basis of the method described in Section "The Dissociation Model", were found to be $N_{\max} = 113$ and $\varphi = 0.90$, respectively. Regarding SAXS, the SLDs (calculated as shown in Section "Scattering Length Densities") and expressed in 10^{-6} Å^{-2} units) of water, HSA, citrate anion and gold are $\rho_{\mathrm{W}} = 9.4$, $\rho_{\mathrm{L}} = 11.9$, $\rho_{\mathrm{F}} = 14.6$ and $\rho_{\mathrm{M}} = 130.7$, respectively, which scale as 1:1.3:1.6:14.0. It

is clear that the high SLD of gold will dominate over the other NP domains, leading to a SAXS form factor $P_{\mathrm{NP}}(q)$ weakly depending on the amount of attached proteins. This framework dramatically changes in the case of SANS using pure D_2O ($x_{\mathrm{D}} = 1$, corresponding to the maximum reduction of incoherent scattering effects[38]): the calculated SLDs of the different NP domains (always in 10^{-6} Å^{-2} units) are much similar, $\rho_{\mathrm{W}} = 6.4$, $\rho_{\mathrm{L}} = 3.1$, $\rho_{\mathrm{F}} = 4.8$ and $\rho_{\mathrm{M}} = 4.5$, with SLD ratios 1:0.5:0.8:0.7. Hence, one might expect that SANS experiments in D_2O are much more sensitive than SAXS experiments to revealing the structure of NPs with protein corona, also at low values of the protein-to-metal ratio ($\bar{r} = C_{\mathrm{L}0}/C_{\mathrm{M}0}$). A deeper investigation of this issue is reported in the Supporting Information (Section "Comparison between SAXS and SANS sensitivities to thermodynamic parameters" and Figure S5).

On the other hand, the high signal-to-noise ratio of SAXS curves that may be collected at synchrotron facilities (in particular at large q values) would make it possible to reveal precisely, at high $\bar{r}$ values, the amount of free proteins in solution, the protein form factor $P_{\mathrm{L}}(q)$ at high q being more intense than the Porod-like decay of the NPs' form factor $P_{\mathrm{NP}}(q)$.[37] On these grounds, it is expected that a combination of SAXS experiments at high $\bar{r}$ and SANS experiments at low $\bar{r}$ in heavy water together with SANS experiments at different concentrations of solely proteins in heavy water provides the optimal host of measurements from which structural and thermodynamic features of protein corona NPs can be extracted. To substantiate this picture, we have then simulated six sets of twelve SAS curves each; four SAXS and four SANS curves with NPs and HSA, and four SANS curves with only HSA. The concentration values pertinent to each curve in the different sets are reported in Table 1. Since the concentrations of NPs and HSA are of the order of nM and μM, respectively, the approximation of allowing only for the protein-protein structure factor (Equation 5) holds true. Each set of simulated curves (a-f) is defined by proper values of reference Gibbs free energy ΔG° and cooperative index n, according to the "Set parameters" headline reported in Table 2. A flat background $B = N_A \sum_i C_i b_{i\,\mathrm{inc}}^2$, calculated on the basis of the molar concentration C_i of any i-atom and on its incoherent neutron scattering length $b_{i\,\mathrm{inc}}$, has been

added to the SANS curves. The sets e and f exhibit a low value of the dissociation constant $K_D = 0.8$ μM, representing the regime of a hard corona interaction.[50]

Table 1: HSA, gold and NP concentrations, protein-to-metal ratios and incoherent backgrounds assumed for the simulations of SAXS and SANS data.

#	C_{L0} (μM)	C_{M0} (mM)	C_{NP0} (nM)	$\bar{r}$	B (10^{-4} cm^{-1})
			SAXS		
1	0	0.20	0.22	0	–
2	27	0.18	0.20	0.15	–
3	50	0.17	0.19	0.30	–
4	69	0.15	0.17	0.45	–
			SANS		
5	0	4.00	4.48	0	1.4
6	7	3.64	4.07	0.002	2.2
7	13	3.33	3.73	0.004	3.0
8	18	3.08	3.45	0.006	3.6
9	7	–	–	–	1.0
10	13	–	–	–	1.8
11	18	–	–	–	2.5
12	100	–	–	–	13.8

According to Equation 2-3, the fractions of association sites occupied by protein molecules, $\bar{Y}$, have been calculated for each set as a function of the concentration of free proteins in solutions, C_L. The results are shown in Figure 1 both in a standard way and as a so called Hill plot. It is worth noticing that the selected values of protein and gold concentrations (red and blue points referred to SAXS and SANS simulations, respectively) together with the corresponding $\bar{r}$ allow to sample quite extensively the behaviour of $\bar{Y}$.

The standard deviations of the simulated curves $\frac{d\Sigma}{d\Omega}_s(q)$ have been calculated using a power law $\sigma(q) = k[\frac{d\Sigma}{d\Omega}_s(q)]^\alpha$, where $k = \varepsilon_1[\frac{d\Sigma}{d\Omega}_s(q_1)]^{1-\alpha}$, ε_1 being the relative error at the first simulated value of the scattering vector modulus, q_1. The selected values were $\alpha = 0.75$ and $\varepsilon_1 = 0.03$. To simulate experimental uncertainties, the SAS intensities have been sampled in 400 q points in the q range $8 \cdot 10^{-3}$-0.5 Å^{-1} and each intensity has been randomly moved by sampling from a Gaussian distribution with standard deviation $\sigma(q_i)$. The four sets of simulated curves are shown in Figure 2, panels a-f, together with their best fitting curves

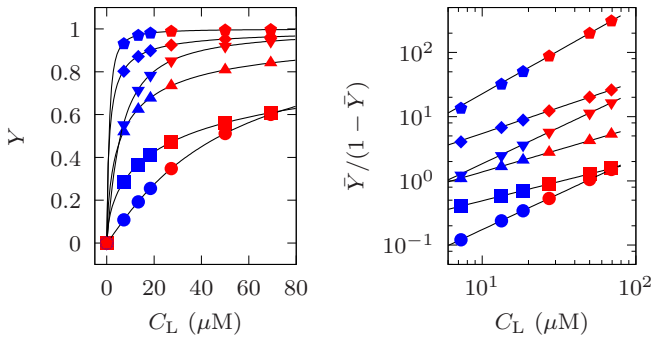

Figure 1: Left frame: fraction of association sites occupied by protein molecules calculated by Equation 2 for HSA and gold concentrations (C_{L0} and C_{M0}) reported in Table 1 and for Gibbs free energy and cooperativity index (ΔG° and n) referring to the six simulations a (circles), b (squares), c (upside-down triangles), d (triangles), e (diamonds) and f (pentamers) according to Table 2, plotted as a function of the in-solution free protein concentration (Equation 3). Red and blue symbols refer to SAXS and SANS curves, respectively. Right frame: same data in the Hill plot representation.

(solid black lines). The fit parameters are reported in Table 2: their standard deviations were determined by repeating 50 times the global fit analysis over the SAS patterns $\frac{d\Sigma}{d\Omega}_s(q_i)$ obtained by randomly sampling from Gaussians with standard deviations $\sigma(q_i)$.

Tiny differences, almost negligible, can be seen among the curves in the different sets, in particular in the SANS curves. However, the best fitting parameters are very close to the values selected in the simulated curves, with an acceptable degree of uncertainty. In detail, structural parameters such as radius and radial dispersion are fitted with a relative error of the order of $\approx 1\%$, whereas Gibbs free energies and cooperative indexes are determined within $\approx 10\%$ uncertainty. Test cases (data not reported) have shown that only a combination of SAXS and SANS data makes it possible to determine with this level of precision the thermodynamic features of the protein-NP dissociation process.

Results and Discussion

The synthesis of Au NPs and their basic physico-chemical properties are fully described in the Supporting Information (Section "Nanoparticles synthesis and characterisation"). The

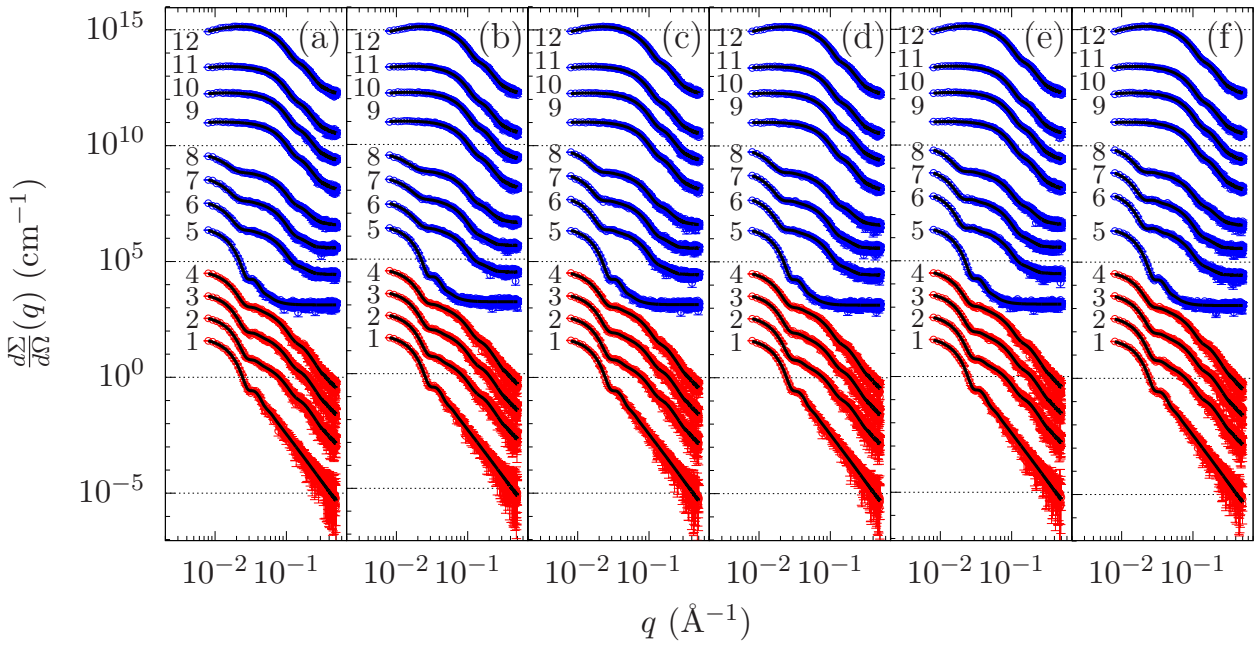

Figure 2: Sets of simulated SAXS (red symbols) and SANS (blue symbols) curves and best fit curves (black solid lines) obtained by the global fitting analysis of each set. Curve labels correspond to the sample conditions reported in Table 1. The stacking factor of the plot is 10. Curve #5 (#9) is offset by a factor 10^4 (10^2) with respect to curve #4 (#8).

Table 2: Best fit parameters obtained by the global fit analysis of four batches of simulated SANS and SAXS curves. Simulation sets a-f are the same as in Figure 2. [a]Derived parameters

			Simulation set					
			a	b	c	d	e	f
Set parameters								
ΔG°		(k_BT)	10	10	12	12	14	14
K_D	[a]	(μM)	45	45	6.1	6.1	0.8	0.8
n			0.7	1.2	0.7	1.2	0.7	1.2
Fitting parameters								
χ^2	[a]		1.07	1.03	1.01	1.07	1.07	1.05
ΔG°		(k_BT)	10.3±0.4	9.9±0.4	12.0±0.1	12.1±0.2	13.6±0.6	13.8±0.5
K_D	[a]	(μM)	30±10	50±20	6.3±0.9	6±1	1.2±0.7	1.0±0.5
n			0.60±0.07	1.1±0.2	0.70±0.07	1.1±0.1	0.8±0.3	1.3±0.2
$<R>$		(Å)	149.8±0.6	148.8±0.3	149.9±0.4	149.0±0.4	149.8±0.5	150.0±0.2
ξ			0.151±0.004	0.151±0.003	0.151±0.003	0.154±0.003	0.150±0.003	0.151±0.002
ϱ_W			1.051±0.002	1.0509±0.0006	1.049±0.002	1.049±0.001	1.051±0.002	1.050±0.001
t_2		(Å)	33±3	32±3	33±3	34±3	34±3	30±2
a_L		(Å^2)	3400±400	2600±400	2800±100	2900±300	2800±200	2500±100
N_{max}	[a]		90±10	120±10	112±5	110±10	113±5	126±5
D		(Å)	60±2	62±2	60±3	62±3	63±3	60±2
z		(e)	−4.2±0.1	−4.19±0.07	−4.0±0.1	−4.0±0.1	−4.3±0.1	−4.0±0.1
I_S		(μM)	100±40	69±8	10±40	60±20	80±40	0±40
J		(k_BT)	11±9	16±4	14±3	16±8	21±5	18±7
d		(Å)	5±2	4±2	4±2	4±3	3±2	3±2

experimental features of SAXS and SANS measurements are as well reported in the Supporting Information (Sections "SAXS experiments" and "SANS experiments", respectively). It is noteworthy that, firstly, the ratio between the molar concentration of HSA and NPs is in the order of 10^6 and 10^4 for SAXS and SANS, respectively, and, secondly, that the maximum value of the HSA volume fraction is 0.66% for SAXS and 0.093% for SANS. Hence, the approximation of taking into account only the protein-protein structure factor (Equation 7) is suitable.

The strategy for data processing in this work aims at treating all the sets of data by using a single model, while keeping the number of fitting parameters at a minimum. According to this picture, only a few free parameters should be optimised in order to fit with a unique analysis the whole ensemble of SAXS and SANS curves in the full q range.

The main structural parameters are the average radius $< R >$ of bare NPs and its log-normal dispersion ξ. Since SAXS and SANS samples have been obtained via two different preparations, in H_2O and D_2O respectively, with possible variations of NPs' size polydispersion, we have optimized two values of $< R >$ and two values of ξ, corresponding to each preparation. A unique thickness of the citrate shell has been assumed and fixed to the same value, $t_1 = 7.2$ Å, selected for the simulations.[51] The thickness of the second layer (t_2) is a fit variable that has been set free to float between the height of the triangular prism[16] that better represents the shape of the HSA molecules (estimated to be as large as 34 Å) and the diameter of the sphere with a volume equal to the volume of a dry HSA molecule ($t_2 = (6\nu_{\mathrm{L}}/\pi)^{1/3}$) that was found to be 54 Å. Accordingly, the surface a_{L} of one protein molecule "box" attached to the NP has been optimized between 2500 and 3500 Å^2. Remarkably, the maximum number of protein association sites (N_{max}) depends on the average bare radius and its dispersion (that have distinct values for SAXS and SANS series) and on a_{L}. Another structural fitting parameter is the relative mass density d_{W} of water in the first hydration shell of the free HSA molecules in the solvent, which is considered a common parameter for both SAXS and SANS batches of data.

Concerning the SLDs of the solvents and of the different NP domains (ρ_α with $\alpha = \mathrm{M, F, L, W}$), the values discussed in the Section "Validation of the Method" have been used. For SANS data from NPs, the deuteration grade has been calculated from the deuteration grade of the stock NP solutions, x_{DM}, according to $x_{\mathrm{D}} = (x_{\mathrm{DM}} V_{\mathrm{NP}} + V_{\mathrm{L}})/(V_{\mathrm{NP}} + V_{\mathrm{L}})$, where V_{NP} and V_{L} are the two volumes of NP and HSA stock solutions mixed. We have then considered x_{DM} as a further optimising parameter and assumed that the HSA stock solution has a deuteration grade of unity. As to the SANS curves of the HSA samples without NPs (see Figure 3(c)), further fitting parameters pertaining the protein-protein structure factor $S_{\mathrm{LL}}(q)$ are the average protein diameter D, the protein net charge z, the added ionic strength I_S, the depth at the contact and the range of the attractive potential, J and d. Importantly, the fitting parameters of the HSA form factor $P_{\mathrm{L}}(q)$ are shared among all SAXS and SANS curves with and without NPs.

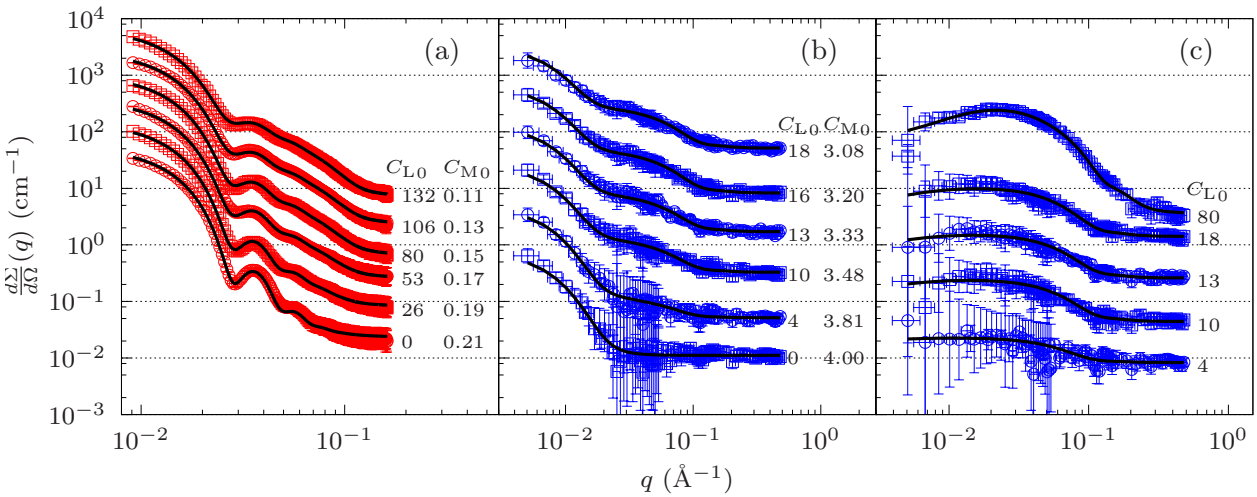

Figure 3: Experimental and fitted SAXS and SANS data of gold NPs in the presence of HSA. Total molar concentrations of HSA, C_{L0}, and gold, C_{M0}, are reported next to each curve in μM and mM units, respectively. Solid black lines are the best fit curves obtained by GENFIT. a) SAXS data of NPs in the presence of HSA recorded at ESRF. Curves are stacked by a factor 3 for sake of clarity. b) SANS data of D_2O solutions of gold NPs in the presence of HSA. Curves are stacked by a factor 5 for sake of clarity. c) SANS data of HSA in D_2O solution recorded at LLB. Curves are stacked by a factor 5 for sake of clarity. The length of the horizontal bar shown for each q of all SANS data represents twice the experimental standard deviation σ_q.

As widely discussed in the Section "SAS Model of Protein Coated Nanoparticles", the fundamental thermodynamic parameters describing the dissociation of HSA from gold NPs and shared among all SAXS and SANS curves are ΔG° (optimized in the wide range 1-100 k_BT) and the cooperative index n.

All these parameters are in common with all the samples because they do not depend on the total amount of gold ($C_{\mathrm{M}0}$) or HSA ($C_{\mathrm{L}0}$) in the samples. On the other hand, considering incoherent scattering effects, each SANS curve is fitted also using a proper background B. Moreover, in the case of SANS, the calculated $\frac{d\Sigma}{d\Omega}(q)$ have been convoluted with the resolution function (see Equation 8) calculated through Equations 33 and 34 of Pedersen et al. [46] on the basis of the standard deviations σ_q experimentally available for each q-channel. The integral in Equation 8 has been numerically calculated using the trapezoidal rule over a grid of 15 points.

The best fit results of all SAS data are shown in Figure 3 (frames a-c). All fitting parameters, apart from the backgrounds B, are reported in Table 3 and their standard deviations have been estimated following the same strategy explained for the analysis of the simulated curves. We have also calculated the correlation matrix among the parameters (see Supporting Information, Figure S6): results indicate the absence of any significant correlation.

The quality of data fitting appears to be quite high, with an average χ^2 as large as 1.04. Clearly, the most relevant parameters are the unique values of the free energy difference ΔG° that assists the dissociation process of one HSA molecule from the NP surface and the Hill cooperative index n. The small value $\Delta G^\circ/(k_BT) = 11.0 \pm 0.5$ means that the corona formed by HSA on gold NPs is a soft corona, according to Lundqvist et al. [50] The dissociation constant related to ΔG° is found to be $K_D = 17 \pm 8$ μM: within the uncertainty interval, this finding is in good agreement with results of Röcker et al. [16] and the most recent findings of Bekdemir and Stellacci [20]. Moreover, the cooperative index obtained is significantly lower than one ($n = 0.8 \pm 0.1$), indicating, in agreement with Röcker et al. [16] and Capomaccio

Table 3: Common fitting parameters obtained for the SAXS and SANS curves reported in Figure 3. [a] Derived parameters. [b] Parameters of SAXS curves. [c] Parameters of SANS curves.

χ^2	[a]		1.04
ΔG°		(k_BT)	11.0±0.5
K_D	[a]	(μM)	17±8
n			0.8±0.1
$<R>$	[b]	(Å)	154.6±0.2
ξ	[b]		0.101±0.002
$<R>$	[c]	(Å)	145±9
ξ	[c]		0.35±0.04
a_{L}		(Å^2)	3200±400
N_{max}	[a,b]		100±20
N_{max}	[a,c]		100±30
t_2		(Å)	30±3
x_{DM}			0.981±0.006
d_{W}			1.081±0.007
D		(Å)	63±4
z		(e)	−4.2±0.2
I_S		(μM)	50±20
J		(k_BT)	30±1
d		(Å)	3.1±0.4

et al.[26], a certain degree of steric hindrance to the binding of other protein molecules to the NP surface after the binding of the first ones.

The area occupied by a single HSA molecule when associated with the gold NP, $a_{\mathrm{L}} = 3200 \pm 400$ Å^2, and the protein layer thickness, $t_2 = 30 \pm 3$ Å, show that the HSA-NP interface mainly involves the basis of the triangular prism approximating the protein shape.

For both SAXS and SANS series, the average NP radii are very close to the nominal value of 150 Å, however a quite high difference is stated in their log-normal dispersions ξ, i.e. 0.101 ± 0.002 for SAXS and 0.35 ± 0.04 for SANS. We can attribute this difference, which is however in agreement with the size distribution obtained with TEM, DLS and CLS (see Supporting Information, Figure S1-S4 and Table S1) to possible batch-to-batch variations.

Among the derived parameters, focus should be brought in the maximum number of protein sites N_{max}, which represents a higher limit for the stoichiometry of the NP-protein

association: similar results for all SAXS and SANS patterns were obtained, i.e. 100 ± 20 and 100 ± 30, respectively.

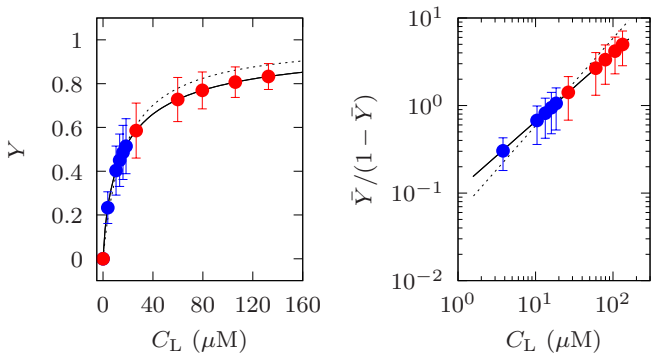

Figure 4: Left frame: fraction of association sites occupied by protein molecules obtained by the global fit analysis of experimental SAXS and SANS curves for gold NPs in the presence of HSA plotted as a function of the in-solution free protein concentration. Red and blue circles refer to SAXS and SANS data, respectively. The solid black lines feature the trend calculated via Equation 2 and 3 for values of ΔG° and n obtained by data fitting. The dashed black lines represent the trend for the same value of ΔG° and for $n = 1$. Right frame: same data as a Hill plot.

The trend of the fraction of association sites occupied by protein molecules, $\bar{Y}$, is plotted in Figure 4 versus the free protein in solution, C_L, after model fitting in the standard form (left frame) and as a Hill-plot form (right frame). The data points, with the derived error bars, refer to different ranges of protein concentration probed via SAXS (red points) and SANS (blue points). The solid black lines are the theoretical solutions of Equation 2 and 3 with the numerically optimized parameters. The dashed line describes the trend of $\bar{Y}$ with the same values of ΔG° obtained through the fit but with $n = 1$. Within the derived error bars, it is clear that from the experimental framework of the presented SAS data, estimating a cooperative index lower than 1 can be seen as a robust achievement.

The best fit parameters relevant to the protein-protein interaction in solution (effective protein diameter D, protein net charge z, added ionic strength I_S and depth and range of the attractive potential, J and d, respectively) are in full agreement with the literature results of HSA in neutral pH.[49]

As final remarks, we wish to underline that the stability of the fitted parameters has

required SAS measurements in absolute units, and the nominal concentrations of gold and of HSA to be kept fixed to the values originating from sample preparations.

Conclusions

We have demonstrated that whole sets of SAXS and SANS data can be simultaneously processed for studying the structure and thermodynamics of proteins associated with NP surfaces. The strategy has been to collect a sequence of SAS patterns by varying the concentration of protein and NPs. Then, the whole set of data has been analysed: we tested this approach on the interaction of Au NPs with HSA, finding that the process is described according to the Hill model of dissociation. In particular, equations 2 and 5 represent the functions against which the data sets are fitted. These equations contain as main parameters the Hill constant and the cooperative index that describe[34] the dissociation equilibrium between HSA molecules and Au NPs. The thermodynamics of the process is characterised by i) the ΔG° free energy: the value obtained from the data best fits nicely suggests the formation of a soft corona, and ii) the n parameter of the Hill model; a figure of 0.8 ± 0.1 was obtained, clearly indicating that the adsorbtion of one protein molecule on the NP surface moderately depresses the affinity for the association of other protein molecules.

The structure of NP interacting with HSA is well modelled by a three density level sphere. The inner core is the Au NP, being covered by an intermediate layer of capping citrate anions; the outer layer is a monolayer of HSA: we found that for 300 Å Au NPs, the formation of the HSA monolayer is consistent with the association of ≈ 100 molecules. The stoichiometry of the nanoparticle-protein complex is therefore established. We also remark that the best fit of the whole set of SANS patterns from HSA solutions without NPs has been essential for improving the stability of the fitting procedure and hence the soundness of the fit parameters underlining the NP-protein association mechanism.

Two further comments are due concerning the results presented. First, we note that both

SAXS and SANS experiments were performed on Au NPs without any previous treatment. To this respect, the method proposed compares favourably with, e.g., fluorescence correlation spectroscopy experiments[16] requiring the NPs to be fluorescent and therefore the insertion of organic fluorophores in the capping layer of nonfluorescent NPs. Second, it is known that different proteins have different dissociation constants for a given NP. This simple fact is the origin of the Vroman effect:[52] mobile proteins arrive first at the NP surface and adsorb, but are then replaced by less mobile proteins having higher affinities. At the end of the process, the protein corona is so strongly bound that zero concentration of free protein in solution is detected when the particle is removed from the biological environment and placed in pure water. For this reason, the nanoparticle-protein interaction is often deemed to be irreversible. We remark that, in agreement with previous literature but on different NPs,[16] the dissociation constant we found for HSA towards gold nanoparticles is 17 ± 8 μM, pointing towards the formation of a soft corona and therefore a mild equilibrium between adsorbed and free protein molecules in solution. To further confirm that this is not an artifact induced by our initial assumptions, we have computed sets of SANS and SAXS curves in the limiting condition of very low dissociation constant, i.e. 0.8 μM (see Table 2, sets e and f). When these calculations are compared to our experimental results (see Supporting Information, Figure S7), appreciable differences are detected. In addition, as shown in validation tests reported in Figure 2 and Table 2 (sets e and f), if statistical noise is added to simulated curves and then these are fitted against our model, a dissociation constant as low as 1.2 ± 0.7 μM (set e) or 1.0 ± 0.5 μM (set f) is retrieved. Taking into account the above remarks, our method could in principle be applied to any system.

We finally remark that both SANS and SAXS data in this work were collected under physiological conditions. This paves the way for *in-situ* and *in operando* studies of the complex problem of NP-protein association.

Supporting Information Available

Nanoparticles synthesis and characterisation; SAXS experiments; SANS experiments; Comparison between SAXS and SANS sensitivities to thermodynamic parameters; TEM pictures and derived size distributions of as prepared Au NPs (Figure S1); UV-Vis spectra of the as prepared Au NPs (Figure S2); DLS size distributions of Au NPs (Figure S3); CLS size distribution in weight of Au NPs (Figure S4); Physico-chemical parameters of the AuNPs (Table S1); Divergence of SAXS and SANS curves of gold NPs in the presence of HSA as a function of the protein-to-metal ratio $\bar{r}$ (Figure S5); Correlation matrix of common fitting parameters (Figure S6); Comparisons between best fit curves and curves with K_D fixed to 0.8 μM (Figure S7).

This material is available free of charge via the Internet at `http://pubs.acs.org/`.

References

(1) Vance, M. E.; Kuiken, T.; Vejerano, E. P.; McGinnis, S. P.; Jr., M. F. H.; Rejeski, D.; Hull, M. S. Nanotechnology in the Real World: Redeveloping the Nanomaterial Consumer Products Inventory. *Beilstein J. Nanotechnol.* **2015**, *6*, 1769–1780.

(2) Liu, R.; Jiang, W.; Walkey, C.; Chang, W. C. W.; Cohen, Y. Prediction of Nanoparticles-Cell Association Based on Corona Proteins and Physicochemical Properties. *Nanoscale* **2015**, *7*, 9664–9675.

(3) Alcantara, D.; Lopez, S.; García-Martin, M. L.; Pozo, D. Iron oxide nanoparticles as magnetic relaxation switching (MRSw) sensors: Current applications in nanomedicine Nanomedicine. *Nanotechnology, Biology, and Medicine* **2016**, *12*, 1253–1262.

(4) Amstad, E.; Textor, M.; Reimhult, E. Stabilization and functionalization of iron oxide nanoparticles for biomedical Applications. *Nanoscale* **2011**, *3*, 2819–2843.

(5) Alexis, F.; Pridgen, E. M.; Langer, R.; Farokhzad, O. C. Nanoparticle Technologies for Cancer Therapy. *Handbook of Experimental Pharmacology* **2010**, *197*, 55–86.

(6) Suarato, G.; Li, W.; Meng, Y. Role of pH-responsiveness in the design of chitosan-based cancer nanotherapeutics: A review. *Biointerphases* **2016**, *11*, 04B201.

(7) Nel, A.; Xia, T.; Madler, L.; Ti, N. Toxic Potential of Materials at the Nanolevel. *Science* **2006**, *311*, 622–627.

(8) Sharifi, S.; Behzadi, S.; Laurent, S.; Forrest, M. L.; Stroevee, P.; Mahmoudi, M. Toxicity of Nanomaterials. *Chem. Soc. Rev.* **2012**, *41*, 2323–2343.

(9) Khorasani, A. A.; Weaver, J. L.; Salvador-Morales, C. Closing the Gap: Accelerating the Translational Process in Nanomedicine by Proposing Standardized Characterization Techniques. *Int. J. Nanomed.* **2014**, *9*, 5729–5751.

(10) Lin, P.-C.; Lin, S.; Wang, P.; Sridhar, R. Techniques for Physicochemical Characterization of Nanomaterials. *Biotechnol. Adv.* **2014**, *32*, 711–726.

(11) Castner, D. G.; Grainger, D. Nanobiomaterials and Nanoanalysis: How to Improve the Nanoscience for Biotechnology. *Adv. Mat.* **2008**, *20*, 867–877.

(12) Baer, D. R.; Gaspar, D. J.; Nachimuthu, P.; Techane, S. D.; Castner, D. G. Application of Surface Chemical Analysis Tools for Characterization of Nanoparticles. *Anal. Bioanal. Chem.* **2010**, *396*, 983–1002.

(13) Mohamoudi, M.; Zope, N. B. H.; Farokhzad, O. C. Emerging understanding of the protein corona at the nano-bio interfaces. *Nanotoday* **2016**, *11*, 817–832.

(14) Walczyk, D.; Bombelli, F. B.; Monopoli, M. P.; Lynch, I.; Dawson, K. A. What the Cell Sees in Bionanoscience. *J. Am. Chem. Soc.* **2010**, *132*, 5761–5768.

(15) Lynch, I.; Salvati, A.; Dawson, K. A. Protein-Nanoparticle Interactions: What Does the Cell See? *Nature Nanotechnology* **2009**, *4*, 546–547.

(16) Röcker, C.; Pötzl, M.; Zhang, F.; Parak, W. J.; Nienhaus, G. U. A Quantitative Fluorescence Study of Protein Monolayer Formation on Colloidal Nanoparticles. *Nature Nanotechnology* **2009**, *4*, 577–580.

(17) Turci, F.; Ghibaudi, E.; Colonna, M.; B. Boscolo, I. F.; Fubini, B. An Integrated Approach to the Study of the Interaction Between Proteins and Nanoparticles. *Langmuir* **2010**, *26*, 8336–8346.

(18) Winzen, S.; Schoettler, S.; Baier, G.; Rosenauer, C.; Mailaender, V.; Landfester, K.; Mohr, K. Complementary Analysis of the Hard and Soft Protein Corona: Sample Preparation Critically Effects Corona Composition. *Nanoscale* **2015**, *7*, 2992–3001.

(19) Casals, E.; Pfaller, T.; A. Duschl, a. V. P., GJ. Oostingh Time Evolution of the Nanoparticle Protein Corona. *ACS Nano* **2010**, *4*, 3623–3632.

(20) Bekdemir, A.; Stellacci, F. A centrifugation-based physicochemical characterization method for the interaction between proteins and nanoparticles. *Nat Commun.* **2016**, *7*, 13121.

(21) Brewer, S. H.; Glomm, W. R.; Johnson, M. C.; Knag, M. K.; Franzen, S. Probing BSA Binding to Citrate-Coated Gold Nanoparticles and Surfaces. *Langmuir* **2005**, *21*, 9303–9307.

(22) Saha, K.; Rahimi, M.; Yazdani, M.; Kim, S. T.; Moyano, D. F.; Hou, S.; Das, R.; Mout, R.; Rezaee, F.; Mahmoudi, M.; Rotello, V. M. Regulation of Macrophage Recognition through the Interplay of Nanoparticle Surface Functionality and Protein Corona. *ACS Nano* **2016**, *10*, 4421–4430.

(23) Docter, D.; Distler, U.; Storck, W.; Kuharev, J.; Wünsch, D.; Hahlbrock, A.; Knauer, S. K.; Tenzer, S.; Stauber, R. H. Quantitative profiling of the protein coronas that form around nanoparticles. *Nature Protocols* **2014**, *9*, 2030–2044.

(24) Giri, K.; Shameer, K.; Zimmermann, M. T.; Saha, S.; Chakraborty, P. K.; Sharma, A.; Arvizo, R. R.; Madden, B. J.; D. J. Mccormick, J.-P. A. K.; Bhattacharya, R.; Mukherjee, P. Understanding Protein-Nanoparticle Interaction: A New Gateway to Disease Therapeutics. *Bioconjug. Chem.* **2014**, *25*, 1078–1090.

(25) Rahman, M.; Laurent, S.; Tawil, N.; Yahia, L.; Mahmoudi, M. *Protein-Nanoparticle Interactions: The Bio-Nano Interface*; Springer series in Biophysiscs: Springer-Verlag, Heidelberg, 2013; Vol. 15.

(26) Capomaccio, R.; Jimenez, I. O.; Colpo, P.; Gillil, D.; Ceccone, G.; Rossia, F.; Calzolai, L. Determination of the structure and morphology of gold nanoparticle-HSA protein complexes. *Nanoscale* **2015**, *7*, 17653–17657.

(27) Marmorato, P.; Ceccone, G.; Gianoncelli, A.; Pascolo, L.; Ponti, J.; Rossi, F.; Salomé,; Kaulich, B.; Kiskinova, M. Cellular Distribution and Degradation of Cobalt Ferrite Nanoparticles in Balb/3T3 Mouse Fibroblasts. *Toxicol. Lett.* **2011**, *207*, 128–136.

(28) Laera, S.; Ceccone, G.; Rossi, F.; Hussain, D. G. R.; Siligardi, G.; Calzolai, L. Measuring Protein Structure and Stability of Protein-Nanoparticle Systems With Synchrotron Radiation Circular Dichroism. *Nano Lett.* **2011**, *11*, 4480–4484.

(29) Wang, L.; Zhang, T.; Li, P.; Huang, W.; Tang, J.; Wang, P.; Liu, J.; Yuan, Q.; Bai, R.; Li, B.; Zhang, K.; Zhao, Y.; Chen, C. Use of Synchrotron Radiation-Analytical Techniques to Reveal Chemical Origin of Silver-Nanoparticle Cytotoxicity. *ACS Nano* **2015**, *9*, 6532–6547.

(30) Wang, W.; Zhang, H.; Kuzmenko, I.; Mallapragada, S.; Vaknin, D. Assembling Bare Au Nanoparticles at Positively Charged Templates. *Scientific Reports* **2016**, *6*, 26462.

(31) Brown, M. A.; Jordan, I.; Redondo, A. B.; Kleibert, A. H.; Wörner, J.; van Bokhoven, J. In Situ Photoelectron Spectroscopy at the Liquid/Nanoparticle Interface. *Surf. Sci.* **2013**, *610*, 1–6.

(32) Spence, J. C. H.; Weierstall, U.; Chapman, H. N. X-Ray Lasers for Structural and Dynamic Biology. *Rep. Prog. Phys.* **2012**, *75*, 102601.

(33) Li, T.; Senesi, A. J.; Lee, B. Small Angle X-ray Scattering for Nanoparticle Research. *Chem. Rev.* **2016**, *116*, 11128–11180.

(34) Spinozzi, F.; Ferrero, C.; Ortore, M. G.; Antolinos, A. D. M.; Mariani, P. GENFIT: Software for the Analysis of Small-Angle X-Ray and Neutron Scattering Data of Macromolecules In-Solution. *J. App. Cryst.* **2014**, *47*, 1132–1139.

(35) Hill, A. V. The Possible Effects of the Aggregation of the Molecules of Haemoglobin on Its Dissociation Curves. *J. Physiol.* **1918**, *40 (Suppl.)*, iv–vii.

(36) Langmuir, I. The Adsorption of Gases on Plane Surface of Glass, Mica and Platinum. *JACS* **1918**, *40*, 1361–1403.

(37) Feigin, L. A.; Svergun, D. I. *Structure Analysis by Small-Angle X-Ray, Neutron Scattering.*; New York, Plenum Press, 1987.

(38) Jacrot, B. The Study of Biological Structures by Neutron Scattering From Solution. *Reg. Prog. Phys.* **1976**, *39*, 911.

(39) Hansen, J. P.; McDonald, I. R. *The Theory of Simple Liquids*; Academic Press, London, 1986.

(40) Pedersen, J. S. In *Neutron, X-rays and Light. Scattering Methods Applied to Soft Condensed Matter*; Lindner, P., Zemb, T., Eds.; North-Holland, 2002; pp 103–124.

(41) Glatter, O.; Kratky, O. *Small Angle X-Ray Scattering*; Academic Press, 1982.

(42) Berman, H.; Henrick, K.; Nakamura, H. Announcing the Worldwide Protein Data Bank. *Nature Structural Biology* **2003**, *10*, 980–980.

(43) Svergun, D.; Barberato, C.; Koch, M. H. J. CRYSOL - a Program to Evaluate X-Ray Solution Scattering of Biological Macromolecules From Atomic Coordinates. *J. Appl. Cryst.* **1995**, *28*, 768–773.

(44) Merzel, F.; Smith, J. SASIM: A Method for Calculating Small Angle Scattering From Explicit-Atom Models. *Acta Cryst. D* **2002**, *58*, 242–249.

(45) Ortore, M. G.; Spinozzi, F.; Mariani, P.; Paciaroni, A.; Barbosa, L. R. S.; Amenitsch, H.; Steinhart, M.; Ollivier, J.; Russo, D. Combining Structure and Dynamics: Non-Denaturing High-Pressure Effect on Lysozyme in Solution. *J. R. Soc. Interface* **2009**, *6*, S619–S634.

(46) Pedersen, J. S.; Posselt, D.; Mortensen, K. Analytical Treatment of the Resolution Function for Small-Angle Scattering. *J. Appl. Cryst.* **1990**, *23*, 321–333.

(47) Sugio, S.; Kashima, A.; Mochizuki, S.; Noda, M.; Kobayashi, K. Crystal Structure of Human Serum Albumin at 2.5 Å Resolution. *Protein Eng.* **1999**, *12*, 439–446.

(48) Svergun, D.; Richard, S.; Koch, M. H. J.; Sayers, Z.; Kuprin, S.; Zaccai, G. Protein Hydration in Solution: Experimental Obbservation by X-Ray, Neutron Scattering. *Proc. Natl. Acad. Sci. USA* **1998**, *95*, 2267–2272.

(49) Barbosa, L. R. S.; Ortore, M. G.; Spinozzi, F.; Mariani, P.; Bernstorff, S.; Itri, R. The Importance of Protein-Protein Interactions on the pH-Induced Conformational Changes of Bovine Serum Albumin: A Small-Angle X-Ray Scattering Study. *Biophys. J.* **2010**, *98*, 147–157.

(50) Lundqvist, M.; Stigler, J.; Cedervall, T.; Berggard, T.; Flanagan, M. B.; Lynch, I.; Elia, G.; KX, K. X. D. The Evolution of the Protein Corona Around Nanoparticles: A Test Study. *ACS Nano* **2011**, *5*, 7503–7509.

(51) Park, J.-W.; Shumaker-Parry, J. S. Structural Study of Citrate Layers on Gold Nanoparticles: Role of Intermolecular Interactions in Stabilizing Nanoparticles. *J. Am. Chem. Soc.* **2014**, *136*, 1907–1921.

(52) Vroman, L.; Adams, A. L.; Fischer, G. C.; Munoz, P. C. Interaction of high molecular weight kininogen, factor XII, and fibrinogen in plasma at interfaces. *Blood* **1980**, *55*, 156–159.

Graphical TOC Entry

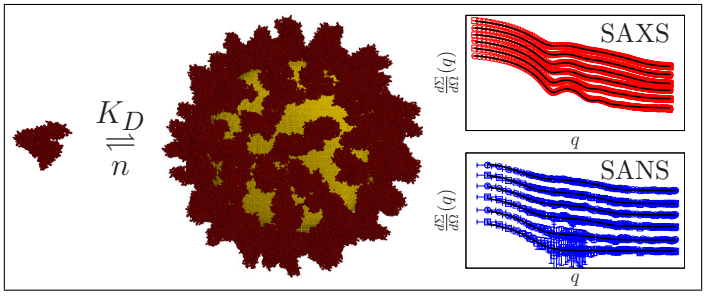

A combination of small-angle X-ray and neutron scattering (SAXS and SANS), analysed with a novel method, simultaneously reveals the structure and the thermodynamics of stabilised gold nanoparticle-protein complexes, according to the Hill cooperative model. The protein dissociation constant, the cooperative index and the stoichiometry of the nanoparticle-protein compound are reliably obtained.